FACTA UNIVERSITATIS
Series: **Mechanical Engineering**
https://doi.org/10.22190/FUME241129002E

Original scientific paper

APPLICATION OF CONCRETE CANVAS FOR ENHANCING RAILWAY SUBSTRUCTURE PERFORMANCE UNDER STATIC AND DYNAMIC LOADS

Balázs Eller[1,2], Szabolcs Fischer[1]

[1]Széchenyi István University,
Department of Transport Infrastructure and Water Resources Engineering, Hungary
[2]University of Pécs, Department of Civil Engineering, Hungary

Abstract. *This study evaluates the potential of Concrete Canvas (CC), a geosynthetic cementitious composite mat (GCCM), in improving railway substructure performance under static and dynamic loads. While CC is widely used for drainage and slope protection, its behavior under railway-specific dynamic forces remains insufficiently studied. Addressing this gap, full-scale laboratory tests, including advanced GOM ATOS 3D scanning and four-point bending evaluations, were conducted to assess deformation, settlement, and shear resistance. Results showed that CC integration reduced settlement by 44.9% compared to unreinforced tracks after one million load cycles, while inner shear resistance can be improved by up to 52-57%. CC's quasi-rigid nature allowed it to withstand over 2.3 million dynamic load cycles – equivalent to 25.875 million tons of mixed traffic – without significant cracking or material failure. The material maintained structural cohesion, with microfractures contributing to its enhanced durability and resistance to deformation. Bending tests revealed that fiber reinforcement in the case of longitudinal weaving direction increased flexural strength by 55.1% after 7 days and 81.7% after 28 days of curing, further emphasizing CC's robustness. These results highlight CC's ability to address issues such as weak subgrades and poor drainage, making it a promising solution for localized track repairs and challenging operational environments. Future research should explore long-term field performance, extreme environmental conditions, and advanced modeling techniques to optimize CC applications in railway infrastructure.*

Key words: *Railway, Ballasted track, Deterioration, Concrete Canvas, CC, Geosynthetic cementitious composite mat, GCCM, Dynamical effect, GOM ATOS*

Received: November 29, 2024 / Accepted January 12, 2025
Corresponding author: Szabolcs Fischer
Department of Transport Infrastructure and Water Resources Engineering, Faculty of Architecture, Civil Engineering and Transport Sciences, Széchenyi István University, H-9026 Győr, Egyetem tér 1., Hungary
E-mail: fischersz@sze.hu

1. INTRODUCTION

Railway tracks are one of the most significant forms of fixed-rail transportation within the domain of land-based travel. Railroads enable the transport of substantial quantities of goods and passengers at relatively high speeds, with low energy consumption and minimal environmental impact (this claim applies predominantly to railways powered by electric traction). For freight transport, longer distances (exceeding 1,000 km) are typically relevant, whereas for passenger transport, shorter distances (generally under 1,000 km) are more significant.

Railway operations rely on the collaboration and contributions of various disciplines, functioning continuously, 24/7. This typically involves a broad range of engineering tasks and their coordination, such as structural designs, load-bearing capacity, and stability (primarily the field of civil engineering [1-7]); the structural configuration and reliable operation of vehicles [8,9]; logistics and traffic management tasks [10-12]; high-voltage traction systems and battery-hybrid systems [13,14]; signaling and safety devices; telecommunications systems; and more.

Railway track structures, whether utilizing traditional crushed stone ballast or ballastless designs, consist of two primary components: the superstructure and the substructure. This article focuses primarily on thin structural elements used at the interface between the ballast and the substructure, exploring their applicability through laboratory testing. Both static and dynamic analyses are considered in this context.

The appropriate drainage and support from the subgrade are essential at the railway structures. Railway track maintenance organizations need solutions that can perform several functions simultaneously and economically. In this case, it means that the operator highly recommended striving for the usage of technologies that can be easily installed and require fewer human and mechanical resources while the solution fulfills the requirements of the renewal. This makes it easy to postpone more serious and expensive interventions, which are necessary but delayed because of the possible cost implications. This deterioration mostly comes from inappropriate drainage, weak subsoil or mudding effect, too. The authors investigate these problems with the experiences of Hungarian State Railways (MÁV) and the Raaberbahn's Hungarian division (ROeEE, i.e., Győr-Sopron-Ebenfurth Railways), but most of the problems can be projected onto the railways of other countries as well.

Following this idea, the authors investigate the application of GCCM (geosynthetic composite cementitious mat) layers in railway circumstances. These materials primarily serve drainage or slope protection purposes; however, the authors see much greater potential in them. Among the GCCM layers, the most promising material is the Concrete Canvas (CC) [15], which was a pioneer in these solutions, was examined. Thanks to the fast early cement curing effect, in addition to good drainage and layer separation, much less installing time and track closure (or, in other words, derail – but not derailment) are necessary. The authors of the current paper (where "authors" is written later in the paper, as it relates to this given meaning) previously made several tests with GCCM material to check the applicability from railway aspects [16,17]. In addition, numerous case studies can be found on the official website of Concrete Canvas [15].

Extreme rainfall and hot weather are no problem. The material is protected against frost damage to a certain extent under the railway ballast, but it is also used for channel lining where there is no frost protection. Thanks to the internal fiber reinforcement and the

double-sided geotextile covering, the material's size change is less; thus, it is much more resistant to frost [15]. In the case of the material suits trench lining, the service life can be extended further with crushed stone covering.

Eller executed research on the behavior of the material under static forces in his previous studies [16-18]. During the research, it was confirmed that the shear resistance showed a more significant effect compared to most types of geogrids [19], which means more stability in the railway ballast. For these types of materials, drainage function is one of the primary solution options; therefore, that solution was not examined separately.

The results proved the applicability, but from a railway point of view, one of the most important parts of these experiments is summarized in this paper. That means the load under a railway track is exceptional. In addition to the dead load, the elements of the track structure suffer and are also subjected to significant dynamic forces. Considering that CC in bond state forms a rigid layer structure, the question arises regarding the behavior of the material under dynamic forces.

It is important to note that the solution is not cost-effective and time-consuming in the case of new construction of longer lengths. On the other hand, the authors believe that the investigated solution is an appropriate possibility for short renewable track sections, where the problem comes from the weak subgrade and the inappropriate drainage.

When the full-scale sample was constructed, the properties of the applied Tensar Triax geogrid were considered according to Al-Sumaiday et al. [20].

As the scope of the CC material is primarily related to the railway topic, it is first necessary to examine the main substructure improvements used in the present. Indraratna et al. [21] showed that the substructure is responsible for the failures of the ballast, which is approx. 58%. The mixing of the materials or the weak subgrade properties causes big problems. Roshan et al. [22] published a review article on railway track degradation, failures, and solutions. The mentioned ground improvement is also discussed by Liu et al. [23], where they discuss the subgrade engineering aspect from the high-speed railway aspect, and by Le Kouby et al. [24], where their approach is generalized in the professional field of railways. Both articles contain ground improvement technologies like geosynthetic-reinforced pile-supported embankments, pile-raft structures and pile-plate structures, or deep mixing. Laboratory studies and field tests were presented by Fortunato et al. [25] about soil-binder columns. The full-scale laboratory measurements presented in this article have inspired the authors' large-scale studies. The traditional reinforcement system, i.e., stabilizations, was collected by Solihu [26]. This review article includes both the advantages and disadvantages of this technology.

In the topic discussed, the number of publications is smaller; what is more, the application of CC in the railway environment is not dealt with by anyone other than the authors. Liu et al. [27] reviewed the design and application of Concrete Canvas reinforced with spacer fabric. The design of the internal fiber structure is also touched upon and is an integral part of this publication, as one of the aims of the paper is to demonstrate the effectiveness of warp-knitted spacer fabric, weft-knitted spacer fabric or woven spacer fabric in improving specific mechanical properties. This solution is not new in industrial applications and has been studied by Zhao et al. [28], while the bending and compression test aspects are discussed considering the ordinary mechanical behavior [29,30]. Ko et al. [31] investigated that regardless of whether or not the blowing agent was added, the bending (flexural) strength tended to increase as the filling factor of the concrete increased, and it was confirmed that the concrete filling rate should be more than 100% to fully exhibit

the physical properties of GCCM. In terms of the characteristics of GCCMs, this may be true for different types of CC materials in general.

The use of Concrete Canvas or GCCMs has many possibilities beyond drainage tasks. As envisioned in its rail application, it can also be used to perform other tasks. One of them is emergency engineering, which is part of the CC material portfolio [32]. Among the many possibilities, tents, underwater pipeline protection, and mine wall reinforcement are among the examples to be mentioned. On the other hand, unique structures were investigated by Mohammadsalehi et al. [33], which were obtained by deforming already solidified materials and joining them as sandwich structures. Joining in a lattice structure increased the flexural strength. Circular concrete columns were covered by a CC layer and tested under axial compression [34,35]. The effect of the reinforcement was significant; compression strength increased by 70-90%. Eller et al. [18] previously performed deflection and other measurements, the application of which will also be part of this article. However, it is necessary to mention [36], which has the same topic in parts. It provides suitable literature for comparing the results.

The ASTM International released several guidelines to help the engineering applications, from which the relevant pieces were taken. In 2018, ASTM International field preparation, layout, installation, and hydration standard of geosynthetic concrete composite mat [37] was published, while in 2019, another guideline was published on the topic of the three-point bending test of GCCMs [38]. The third relevant regulation on the subject was issued in 2021, which was the measurement of the compression strength of the GCCMs [39]. All three requirements were taken into account during the measurements; however, some tests had minor differences due to technical limitations.

Despite the increasing use of geosynthetic materials in railway infrastructure, there is still much to learn about the performance and long-term behavior of CC as a reinforcement solution for railway substructures. While CC has proven effective in applications such as drainage, slope stabilization, and even military construction, its potential under the dynamic loads typical of railway traffic has not been thoroughly explored. Most research to date has focused on static load conditions, offering limited insight into how CC responds to the repeated stresses of moving trains or how well it maintains its structural integrity over time. Additionally, many studies have been confined to small-scale laboratory tests, leaving a lack of real-world data to guide practical applications. Comparisons between CC and more traditional reinforcement methods, such as geogrids, are also scarce, making it difficult for engineers to evaluate their suitability for specific challenges like weak subgrades or poor drainage. This study seeks to fill these gaps by investigating CC's performance under both static and dynamic loading conditions, using full-scale testing and advanced measurement techniques. By addressing these unanswered questions, the research aims to provide a clearer picture of CC's capabilities and expand its role as a reliable and innovative solution in railway engineering.

The structure of the study is as follows: Section 2 deals with materials and methods, Section 3 is about the results and discussion, and Section 4 contains the derived conclusions as so-called "thesis statements".

2. MATERIALS AND METHODS

2.1. Materials

2.1.1. Real-Size (Full-Scale) Tests

In all cases, the same type of stone ballast was applied in current tests. The ballast crushed stone was andesite, with 31.5/50 mm grain sizes (i.e., the nominal minimum grain size was 31.5 mm; hence, the maximum is 50 mm) according to the MSZ EN standard [40]. The sample was given by Colas Északkő Ltd., from the quarry of Szob, Hungary. It can be said that all ten investigations on this topic were made from the same type of stone particles for the correct future comparisons.

In the current article, the CC was purchased from Concrete Canvas Ltd. The dynamical tests were made in 2022 when Concrete Canvas Ltd. modified the composition of the CC. Therefore, the first test was made with type CC13 (where 13 means the thickness of the material in the 'mm' unit); on the other hand, the new tests were made with the newer type CCT3. This is because the manufacturer has modified the structure and reduced the maximum thickness to 11 mm. So, the distributed types nowadays are the CCT1, CCT2 and CCT3 types, where the thicknesses are 5, 7 and 11 mm. These materials are relatively thin compared to the whole layer structure of a railway track. Because of that, these can mainly be compared to geopolymers. There are other notable types of CC, like the CCH or CCX, but thanks to their characteristics, these types are weaker in terms of railway loads.

The protection layer (like in every other measurement) was formed by Z0/22 (0/22 mm) crushed stone. This material was ordered from a local mine near Győr (Hungary). The particle size distribution (PSD) was measured for adequate future comparisons because the significant standard deviation was experienced at the previous measurements. According to PSD, the Z0/22 complies with the normal standard from [41]. The measured PSDs are shown in Fig. 1.

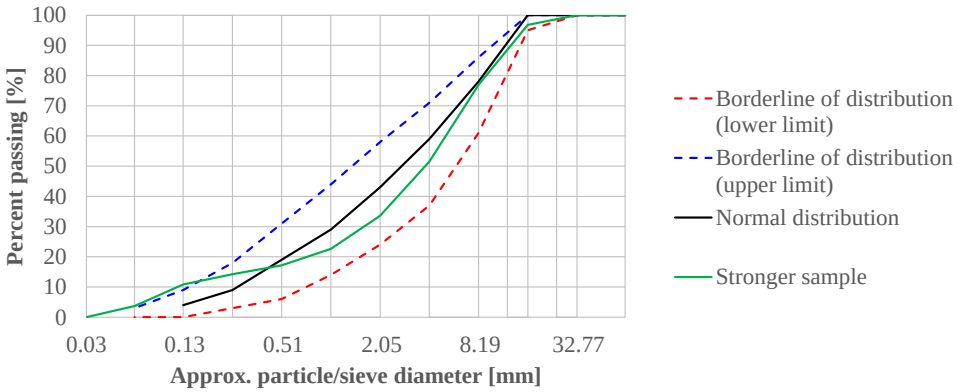

Fig. 1 PSD from the full-scale samples' Z0/22 protection layer
(the applied sieves: 0.032, 0.063, 0.125, 0.25, 0.50, 1, 2, 4, 8, 16, 32, 63 mm)

Permanent displacements and changes were measured using the digital image correlation (DIC) method. The DIC is a widely used non-contact surface deformation

measurement technology; the environmental requirements, while the measurement is simple, the measurement accuracy is high, and it is a widely applicable method [42-47]. Today, DIC measurement is used in many fields of industry and science, including biomechanics, architecture and materials science, but it is not used in railway construction and investigations. This is due to the large number of particles in the railway ballast and the difficulty of accessing them. Nevertheless, it is an excellent solution for representing displacement and deformation in laboratory conditions. In this study, the measurements made by GOM ATOS 3D were combined with GOM TRITOP measurements to increase accuracy. The method was detailed by Szalai et al. [47] and Szalai et al. [48].

In the full-scale sample, an L4 marked (type) MABA Hungaria Ltd. type sleeper was used. Its height is 23 cm, while on the longitudinal aspect, a slice was cut out from the original sleeper. Thanks to this, the length of the sleeper was 39 cm (its centerline is the symmetrical axis of the rail foot), and it follows that the contact area was 29×39 cm^2.

2.1.2. 4-Point Bending and Compression Tests

Eller et al. [18] published the main properties by measurement and evaluation. These results were for specimens that were bonded at rest, without load. The FE (finite element) modeling of the previous bending and compression tests has shown that the 3D fiber reinforcement and fabric covering in the material significantly increases the resistance to the different forces. The aim was to investigate whether this reinforcement could be quantified or not. The cement powder material was not available separately, so the powder was collected from the excess materials that came from previous measurements. Finally, the specimens required for the tests were prepared from the collected cement powder. The specimens prepared were 4×4×16 cm^3 and 7×7×21 cm^3 brick bodies.

On the other hand, another basis for comparison is the examination of the material taken from the full-scale test. In this case, the specimen is given; it has a preloaded, distorted, uneven surface. Thanks to this, the used CC material was mentioned in Section 2.1.1.

2.2. Methods

2.2.1. Real-Size (Full-Scale) Tests

Like the previous investigations on this topic, the tests performed in the laboratory of Széchenyi István University, Győr. This article contains different types of measurements, so these will be presented in two parts. The common parts are the following.

For the dynamical investigation test, a full-scale sample was built under laboratory circumstances. The first try of this test was published by Szalai et al. [49]. Initially, the frame of the sample was made from two layers of wooden sheets/boards, while the filler material was simple sandy gravel with low E_2=16.33 MPa bearing capacity. The measurement was made according to MSZ 2509-3:1989 [50].

After the initial test, the frame was built up from steel U profiles, which ensured 0.25 m thick of 0/22 mm crushed stone protection layer. The thicker protection layer was significant because the sample was built on concrete ground in the laboratory. With this formation, the bearing capacity could be decreased to ensure real circumstances.

The other important part was to decrease the rigidity due to the base layer. To avoid the concrete slab's rigidity, under ballast mats (UBMs) were laid on the base ground. Its thickness is ~3 cm (the average density is 800 kg/m^3, the average hardness on the upper

surface is 44 Shore A, hence on the bottom surface is 46 Shore A; the vertical static bedding modulus is 0.12 N/mm^3, while the vertical dynamic bedding modulus is 0.2 N/mm^3 at 5 Hz and 0.242 N/mm^3 at 10 Hz). On the UBMs, one layer of geotextile was used as a separation layer.

In the 0.25 m thick 0/22 mm protection layer for better bearing capacity, one layer of Triax TX130s geogrid, the effect was studied by Fischer [19]. It was built in the middle of the layer. The protection layer was compacted at 0.12 m and 0.25 m using a 68 kg heavy L-2/C plate vibrator. The size of the plate vibrator is 500×500 mm^2, with a nominal vibration rate of about 3000/min. On the ready layer structure, bearing capacity was measured on the upper plane by static plate load test. The reached bearing capacity was E_2=34.65 MPa, which was a satisfying result from the aspect of the railway loads. This value satisfies the circumstances and conditions for which the authors would apply this solution.

Under the ballast layer, one more geotextile layer was laid to prevent the mixing of the different layers. On the other hand, knowing the contact area of the used sleeper part, the area under the full-scale angle load distribution has been painted out on the white geotextile surface. Editing this "core area" was important because the CC sample had been cut to cover this surface. On the other hand, the edge of the ballast was also signed with orange (color) to ensure an adequate track structure profile. The blue crosses signed the possible dynamic load-bearing capacity measurement points to get appropriate feedback on the homogeneity of the additional layer. It is seen in Fig. 2.

There were 4 measurements with different number measurement cycles. 2 tests were applied with CC and 2 tests without it. These measurements were made in 2022; thanks to this, the applied CC specimen was CC13. The authors decided that between the CC13 and the new type CCT3, the difference is mainly the layer thickness; the experienced behavior will not be modified significantly. That means the results can be compared to the previous measurements.

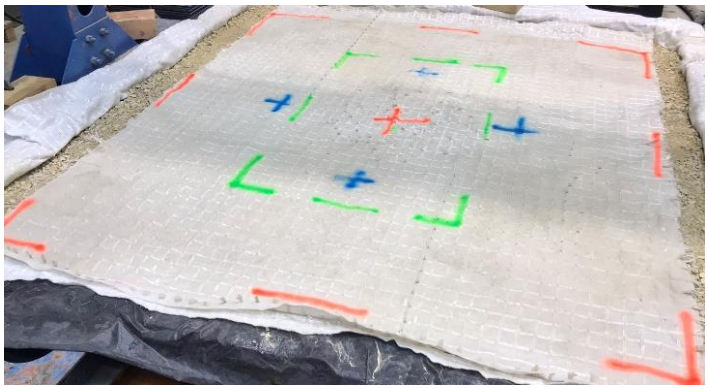

Fig. 2 Set-up of the protection layer, border signs of the materials

The hydration is a critical moment. According to the authors' experience, under laboratory conditions, water easily flowed laterally, so the water had to be collected on the CC surface, while deformation must be minimized. On the other hand, if a lot of water flows out, it is absorbed in the 0/22 mm layer, which can distort the measurements due to

high moisture. The manufacturer's recommendation for hydration for this CC type is 7.5 liter/m^2 of water. The watering was made two times, first directly on the surface of the CC and then on the 10 cm thick ballast layer after the compaction. The amount of water was not measured precisely every time; the addition was approximately as prescribed. It should be noted that CC cannot be overhydrated, so the principle of more rather than less applies. Based on later results, hydration was adequate.

The first GOM ATOS (discussed below, in this section) measurement had to be made on the CC specimen (Fig. 3): the flatness value. The flatness of CC after loading was analyzed [16,17]. After these experiences, the flatness values could be comparable.

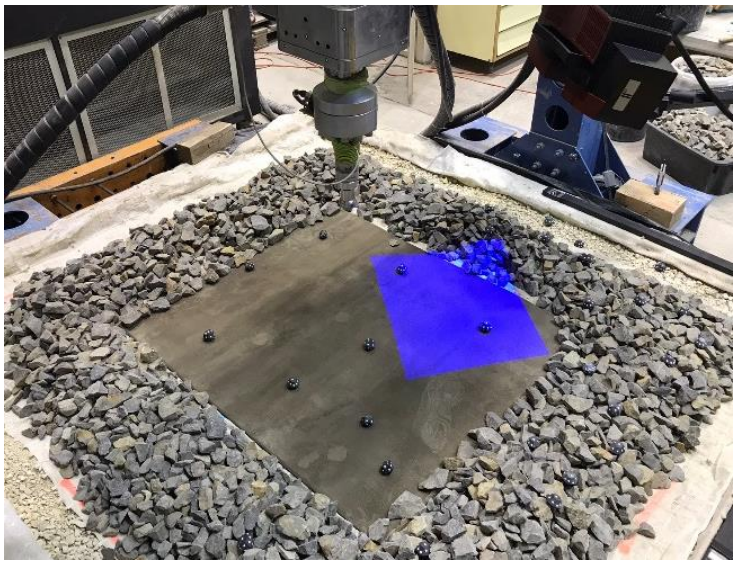

Fig. 3 Flatness measurement before hydration

On the protection layer, the standard nominal ballast thickness was used according to 225 kN axle loads, which resulted in 0.32 m crushed stone with 31.5/50 mm particle size distribution. 0.32 m is also ideal because the structural height of the measuring instrument limited the further increase in ballast bed thickness. The compaction of the railway ballast material was executed in 3 series/phases on each 10 cm height. On the top of the lower ballast layer, a 23 cm height and 39 cm length reinforced concrete sleeper was placed. After that, the ballast was filled until the level of the top of the sleeper. According to the standards, an adequate ballast shoulder was created and compacted.

The final cross-sectional design is shown in Fig. 4.

The best way to measure movements and displacements (i.e., deformation) is to use contactless measurement, one of the modern forms of testing. This 3D technology allows the non-contact measurement of displacements and deformations of objects subjected to mechanical or environmental loads, which is difficult to achieve at a practical level in railway (civil) engineering but can provide excellent results at the laboratory level. The railway ballast and movements, as well as deformations, were measured using the GOM ATOS Triple Scan, a high-precision industrial optical 3D scanner [51-53]. It measures the

entire surface of the part; the two-axis sensor captures a dense point cloud or polygon mesh that accurately describes the geometry of the object, indicating invisible defects. The projector unit projects a pattern of stripes (gray-code-based) of different widths and light intensities onto the object to be immersed, whereby the CCD detects the phase-shifted sinusoidal light intensity variation reflected from the object. These patterns are captured by two cameras [51-53]. The instrument operates on the heterodyne light interference principle, utilizing multiple phase shifts to achieve maximum sub-pixel accuracy. Using the transformation equations of optical imaging, the computer calculates the 3D coordinates of each camera pixel with high precision in just a few seconds.

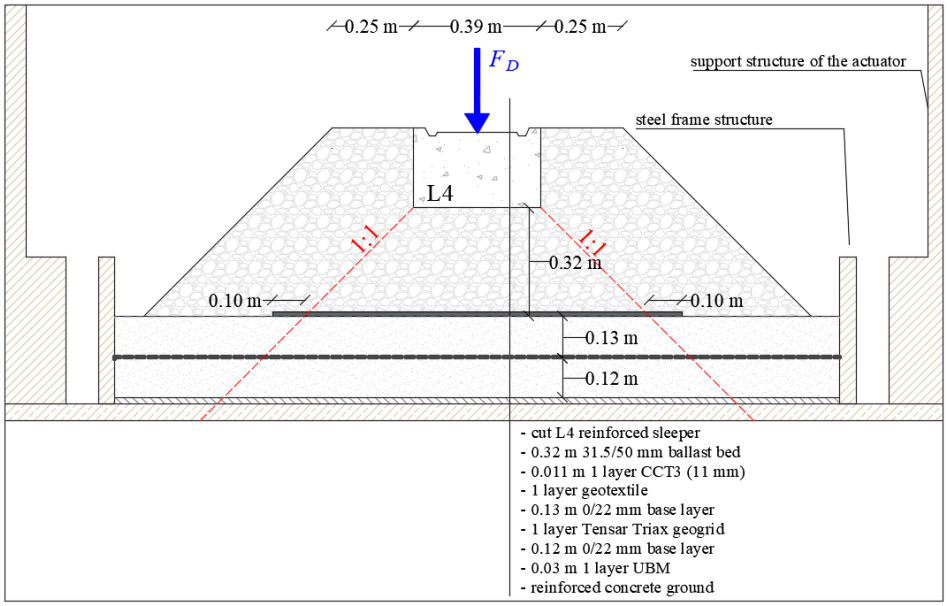

Fig. 4 The set-up of the full-scale test

Multiple independent measurements from different viewpoints are necessary to digitize an object's entire surface. Since both the cameras and the projector are calibrated, 3D surface points can be triangulated from any two of the three distinct views provided by the three units. The projection unit employs low-frequency blue light, which effectively reduces the impact of interfering ambient light [51-53]. The measuring instrument has an accuracy of 17 µm or 0.02 mm. For the measurements, 3D-printed plastic particles (i.e., "eikosi-tessera-eder") are used with point stickers as reference points. These were placed between the variously spaced ballast particles, excluding on the slope or horizontal surface. In addition, point stickers were also glued to the frame of the loading instrument for appropriate measurements. These measurement elements are shown in Fig. 5. With these, the ready full-scale sample; the initial state was measured by GOM ATOS and TRITOP.

Digitization requires system calibration, which involves scanning the caliper plate from various distances and angles. Following the measurement, the scanned models are compared with the CAD model of the original piece using ATOS Professional 2017 software [51-53].

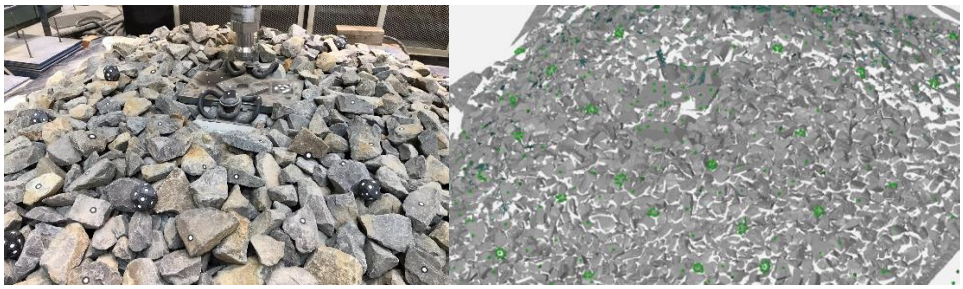

Fig. 5 The reference points in reality (left) and at visualization (right) – green dots, elements

If a cross-section is to be made using the GOM measurement, meshing would be required due to the highly variable and irregular surface of the crushed stone bedding. This would require a significant amount of data, which would require an extensive IT infrastructure. For this reason, the measurement strategy was changed, feature points were selected, and their displacement was taken into account. The GOM TriTop measurement was suitable for this measurement. This measurement was better than a simple geodetic measurement because the specific points are always the same, marked with a marker so that their deformation can be better detected. This method of recording data also allows the displacement of the entire full-scale sample to be investigated since the number of points marked is simply a matter of choice. After the measurement, these can be stored as data and can be easily recalled and compared with other measurements for future analysis. Such a measurement is performed on about 28 to 35 million measurement points, so as mentioned above, an adequate IT background and performance are essential.

After the digitalization, the cyclical dynamical loading was started immediately. This move was significant because the ballast layer needed loading to be pushed into the CC layer. It was a necessary movement to earn the lower stone-cemented state. The full-scale sample was constructed to meet the conditions for an axle load of 225 kN.

The L4 sleeper piece lower plane was 0.29 m wide and 0.39 m long, so the loading area was 0.1131 m^2. To determine the dynamical loading of the device, the calculation method was used from [54]. According to the planned axle load, with these parameters and method, the required dynamic load was $F_{D,max}$=70.83 kN (see Fig. 4).

There were 2 measurements with the CC layer in the structure. GOM measurements were made at the following states: (i) 100,000 cycles, (ii) 200,000 cycles, (iii) 500,000 cycles, (iv) 1.0 million cycles, (v) 2.0 million cycles (only at the first test, due to technical due to technical reasons), (vi) 2.3 million cycles (only at the first test, due of technical due to technical reasons).

After the tests, the sleeper and the ballast were removed. Because of the loading, the particles were pushed into the CC and cemented. The phenomenon was the same as after statical loads. The stone particles had to be removed by force to measure the flatness of the end state. The flatness was measured by GOM ATOS according to the previous investigations.

2.2.2. 4-Point Bending and Compression Tests

As described in Section 2.1.2, the original deflection measurements are compared with unreinforced and preloaded specimens. The considered professional literature and tests were described previously [55-57], like the puncture test, 3-point bending test, tensile test, etc. From that, a four-point bending test, compression strength test and puncture test were made. With the exception of the puncture test, the measurements were repeated with specimens without fiber reinforcement.

The other option is the bending test of CC material with a deformed surface subjected to dynamic loading. In this case, the bending test was planned after the flatness test.

One of the possibilities was the four-point bending measurements after the flatness examination.

The test and the devices were the same as in Eller et al. [18]. 350×200 mm^2 specimens were cut from the 1.1×1.2 m^2 area specimen. The movement of the edges was measured in the middle. It is important to note that each specimen was cut from the 45° nominal loading area only. It is discussed in Section 3.1. The mechanical strength and the volume stability were described by Han et al. [58,59]. As it is known, CC material has two weaving (woven) directions, which show different results in the tests. For this reason, the 12 specimens are divided into 6 pieces per woven direction. In addition to the bending test, it was important to prove that the material did not break under dynamic loading.

The second comparison option is the specimen without 3D fiber reinforcement. A standard specimen shall be used to test the strength properties of concrete, which may be cubic, cylindrical, or slab-shaped. According to this, the authors created 4×4×16 cm^3 and 7×7×21 cm^3 brick bodies (so-called beams) from the aforementioned cement powder. The tested specimen is seen in Fig. 6.

The specimen size was chosen according to the available measuring instruments and the amount of material. First, the smaller specimens were tested in a 3-point bending test; then, a compression test was performed on the intact side. The 3-point bending measurements were discarded due to measurement device errors, but the cubic sections taken from the specimens were usable. So, the compression test corresponded to the compression test of a standard 4×4×4 cm^3 cube. The 7×7×21 cm^3 specimens were measured by 4-point bending tests. According to the previous methods, the specimens were tested after 1, 7, and 28 days of curing.

Fig. 6 The set-up of the four-point bending test and the broken CC specimen

Compressive strength tests were made to calculate the material's Young's modulus (E [MPa]), published by Eller et al. [18]. The specimens were 300×300 mm^2 size tables from CC13. The material was loaded slowly until 200 kN. Thanks to the wide and thin specimen, 200 kN was an upper limit due to the wide and thin material, as a spectacular breakage would hardly ever have occurred in this size dimension. This new compressive strength (destructive) test was carried out according to MSZ EN 206 [60]. During the test, the surface of the pressure plate was larger than the test specimen. The load was applied in a central and uniformly increasing manner. The load was applied until the specimen was destroyed.

The purpose of these methods is to determine to what extent the 3D fiber reinforcement strengthens the material and to what extent the embedded stone particles reduce it. It has to be mentioned that no safety factor was considered in the publishing of strength values.

3. Results and Discussion

3.1. Real-Size Full-Scale Test

As it was mentioned, two measurements were used of CC in the railway structure. First, the number of loaded cycles stopped at 2.3 million, so the simulated mixed mass rolled over is 25.875 million tons. The second test stopped at 800,000 loaded cycles, which means 9.0 million tons. An additional number of cycles was not possible due to instrument failure. In order to compare the adequacy of the samples, a reference measurement was executed. This measurement was taken up to 10 million load cycles, which means 112.5 million through-rolled tons.

As described in the Methods section, GOM measurements were performed after different loading intervals. This data recording method can be used to test the displacement measurement of the entire full-scale sample, about 28-35 million measurement points. In this evaluation, the average heights of the points at the four corners of the sleeper were taken to determine the settlement, and the settlement curve was determined on this basis. The advantage of this measurement is that additional points can be evaluated later on the basis of the test; on the other hand, 3D images and cross-sections can be created, and the point cloud is available.

The recording method can be seen in Fig. 7. In addition to scanning, a number of high-resolution images need to be taken in order to process the data correctly. The measured settlement in each condition can be represented and compared to the previous or initial measurements. In Fig. 8, the full-scale sample's settlement is marked by yellow arrows. The arrows act as vectors, which also show the direction of movement. As mentioned, other fixed points could have been chosen, but the authors focused exclusively on the settling of the railway sleeper.

Using the settlement data from the measurement, the settlement of the sample is presented in Fig. 9. The measured values come from the GOM and the continuous control measurements. Unfortunately, due to technical reasons, the measurement of the full-scale sample with CC ended at 2.3 million load cycles, so someone could only compare it with the sample 10 million load-cycle sample. On the graph, according to the measured settlements, a power function was applied. This fits appropriately to the measured settlements after different amounts of loads. It can be concluded that at 1 million load

cycles, the use of the CC specimen more than halved the settlement of the reference track structure. No further measurements were made for technical reasons. The results can be compared to the ones reported by Fischer [5], where the investigation was related to field tests and measurements. According to [5], tracks behave like logarithmic settlements; however, the current tests showed power functions. This is not a clear and problematic discrepancy, but it does require further investigation, in particular to identify the causes and factors that have modified the curves in the studies related to Section 2.1.1, where both the unreinforced and CC-reinforced designs showed power function settlement trends.

Eller et al. [17] proved that the CC layer can increase the inner shear resistance by 52-57% if the CC layer gets the necessary preloading or normal loading. In these previous tests, there were two options. At first, the layer was loaded by 100 kN for 7 days, while the second series was loaded by 100 kN for only 30 minutes, both statically. As it was emphasized above, the considered samples were loaded immediately after the building.

After removing the ballast layer, the surface of the CC layer was the same as under the static loading tests. The penetration effect of the ballast particles showed the same state, which means the immediate loading on the structure helps to achieve the same results. From this, the same inner shear resistance is estimated.

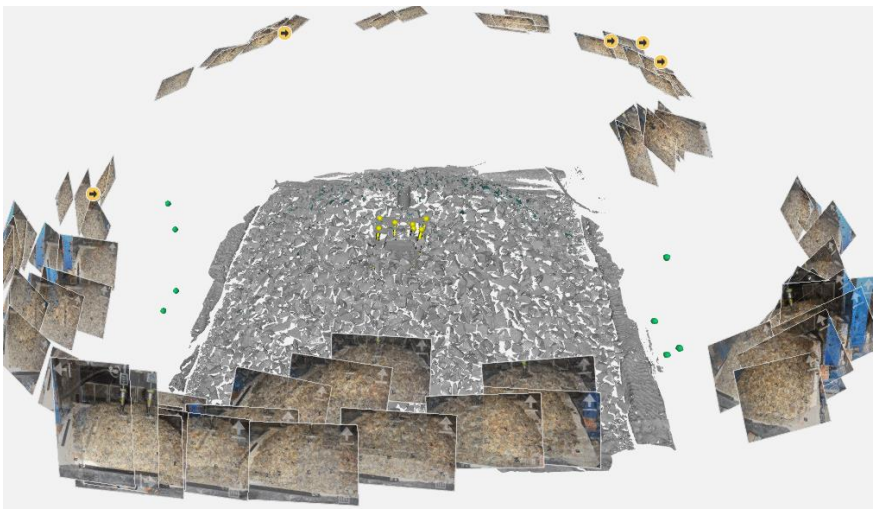

Fig. 7 Scanning, in addition to surround imaging

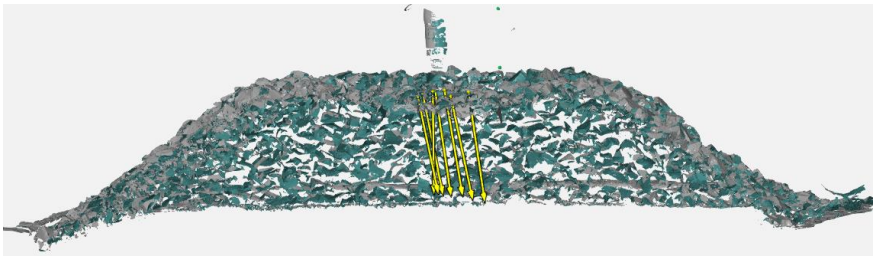

Fig. 8 The state after a given load, representing the rate and vector direction of settling

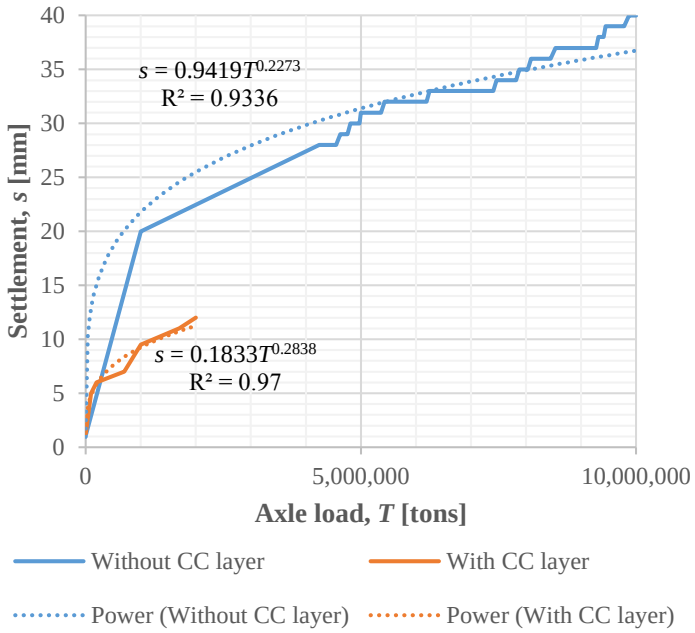

Fig. 9 Comparison of the settlements of the full-scale samples, with and without CC layer in the track structure

The surface was measured by GOM ATOS to compare the penetration between the static and the dynamic loading cases. Before the 3D scanning, all the stone particles had to be removed from the layer structure. In some cases, the particles could be moved only by force. After scanning the surface, it was seen that the flatness value was nearly the same. These results are summarized in Table 1. It is seen that the 7 days of static preloading had a more significant effect on the CC, while the other two options showed similar results. From this, it can be assumed that the dead load alone provides enough load for the ballast particles to penetrate into the CC layer.

Under the sleeper, the deflection was larger a bit, but not significantly (Fig. 10). On the other hand, the unevenness and the penetrations are clearly visible, which is presented in Fig. 10. Due to the compressive force of the particles, the cement powder separated from the CC layer and surrounded the ballast particles. The bonding happened with this deformation.

As was written above, the main question at this solution was the CC's behavior under dynamic loads. At the laboratory, after the sample was removed, it was seen that the CC layer was not cracked/broken. To be able to prove this scientifically, an additional measurement had to be used. According to Section 2.1.2, the CC was cut into pieces (Fig. 11.), and the pieces were measured in a four-point-bending test. Fig. 11 shows the planned cut lines and the cross-sections covered by the 4-point bending measurement (red bar), the number of specimens and the direction of weaving of the specimens. The green edge represents the border of the nominal 45° load distribution.

In the figures and tables given below, the following abbreviations are used: AV stands for ‘average’, SD for ‘standard deviation’, RSD for ‘relative standard deviation’.

Table 1 Comparison of the flatness values, using previous results from [15,17]

Specimens	Hydration	AV flatness [-]	SD flatness [-]	RSD flatness [%]
Before hydration	0 day	12.68	-	-
CC after seven days of permanent 100 kN load	7 days	28.63	5.799	20.30
CC after 30 min. of permanent 100 kN load	7 days	21.08	1.598	7.60
CC in the full-scale sample after immediate dynamic loads	28+ days	20.99	2.660	12.70

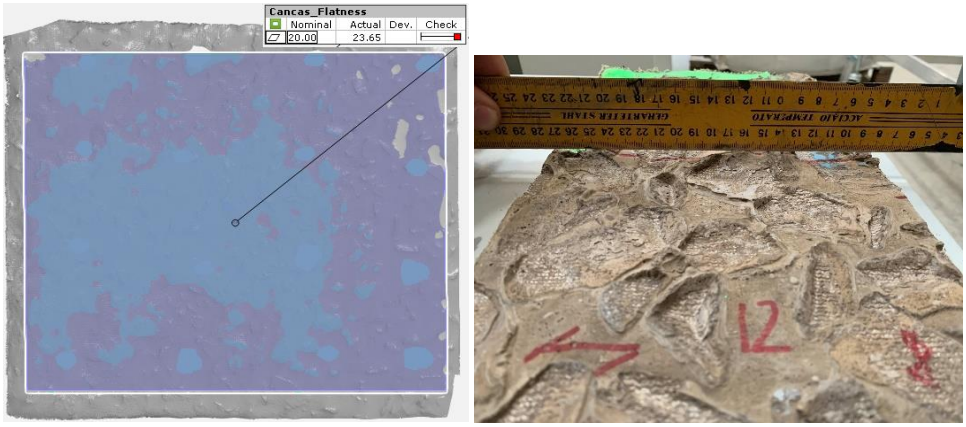

Fig. 10 Scanned CC layer from the full-scale sample after dynamical loads (left), as well as the surface deformation of the cut-out specimen (right)

As a result of the absorbed forces, the specimen resists and breaks, so the authors look for the magnitude of the resistance up to the moment of the first crack. So, if all graphs have the same slope up (i.e., tangent) to a certain point, the material is considered rigid, not broken. If the tangent is much lower than the other specimens, the specimen is considered broken.

The measured bending at the first crack can be seen in Table 2.

In Figs. 12 and 13, it is seen that the steepness of the force resistance is nearly the same in every specimen until a certain amount of loading. After the first cracks had occurred, the loading continued, and then after 9-10 mm bending, the loading was removed. Without loading, the deflection of the specimens "went back". The different directions in the woven fabric showed different final conditions, too. In the longitudinal direction went back to 3.0 mm (±0.5 mm), while in the transversal direction went back to 4.0 mm (±0.3 mm). In the latter case, the standard deviation was more minor.

In summary, the pattern of the graphs has three stages. The first is until the first crack; hence, the third is after removing the loads. These are nearly the same in all specimens. However, in the middle (second) section variable, the slope of the increase in bending is similar. The difference between the flexural strengths was not significant.

The specimens after the test are seen in Fig. 14. Even after the tests, no serious fracture was visible after 9-10 mm of bending; the structure remained intact, so a certain degree of flexibility was ensured. From a railway point of view, this demonstrates that the formation of cracks in slight bending does occur when tearing in the textile or PVC layers. This means that drainage will not be a problem in the event of a breakage under dynamic loads.

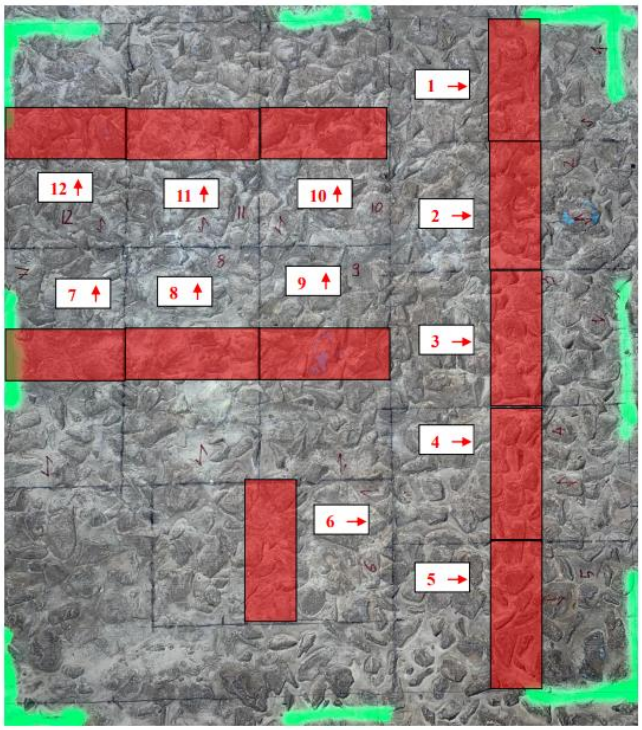

Fig. 11 Plan of the line (direction) of cuts on the dynamically loaded specimen

Table 2 Four-point-bending test results based on force-displacement graphs

	Longitudinal woven	**Transversal woven**
AV load at first crack [kN]	0.260	0.190
SD load at first crack [kN]	0.003	0.026
AV displacement at first crack [mm]	1.990	1.690
SD displacement at first crack [mm]	0.470	0.650

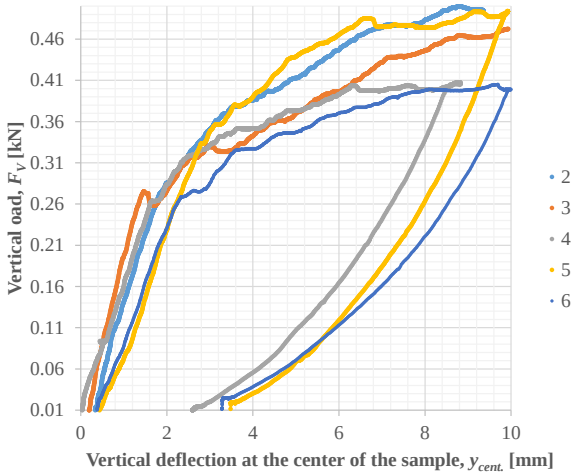

Fig. 12 Results of four-point bending tests with different weavings – longitudinal woven

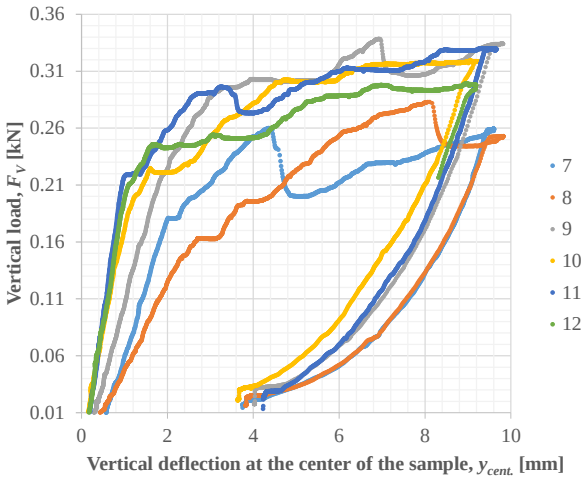

Fig. 13 Results of four-point bending tests with different weavings – transversal woven

Fig. 14 Specimens Nr. 1-6 after the four-point bending test

3.2. 4-Point-Bending and Compression Tests

As mentioned above, one of the aims is to show the difference in deflection between reinforced and unreinforced CC material. The authors assumed, based on measurement and modeling experience, that the mechanical resistance of materials with 3D fiber reinforcement is much higher than that of unreinforced specimens. Thus, as described in Section 2, the specimens were prepared, and measurements were performed.

Measurements of the material taken from the full-scale sample were also taken to complete the measurements. Naturally, a significant variance was expected due to the variable deformation/deposition caused by the bedding particles, but it can be said that throughout the research, the variance was always significant when testing the CC material.

The results of the measurements are summarized in Table 3. The original deflection studies were presented by Eller et al. [18] and are not included in Table 3. In addition to summarizing the measurements of the CC material at 1, 7 and 28 days of curing age, the measurements of the material taken from the full-scale sample were also examined at curing ages older than 28 days. Since the total curing time is 28 days, no distinction was made between specimens "older" than 28 days and specimens 28 days old. The results shown in Table 3 indicate that 3D fiber reinforcement has a significant effect on the bending resistance, but not in all weaving directions. Previous measurements show that there is a significant difference between longitudinal and transversal weaving. This difference is also shown in the same way for the specimen taken from under the stone bedding, but starting from a lower value, so the numerical difference is also smaller. It is also seen that the standard deviation increases as the flexural strength increases. As expected, the standard deviation of the CC material with a deformed surface was more significant than that of the other specimens.

Table 3 Comparing unreinforced and reinforced CC's flexural strengths (fl. str.) with [18] and related deflections until the first crack during 4-point bending tests (long. stands for 'longitudinal', transv. for 'transversal')

CC without 3D fiber results in 1 day (left) and 7 days (right)					
AV fl. str. [MPa]	3.57	not relevant	AV fl. str. [MPa]	3.61	not relevant
SD fl. str. [MPa]	0.39		SD fl. str. [MPa]	0.57	
Diff. from [18]	10.84%		Diff. from [18]	15.86%	
AV $y_{cent.}$ [mm]	2.25		AV $y_{cent.}$ [mm]	1.43	
CC without 3D fiber results in 28 days					
AV fl. str. [MPa]	4.31	not relevant			
SD fl. str. [MPa]	0.76				
Diff. from [18]	17.53%				
AV $y_{cent.}$ [mm]	1.92				
CC from the full-scale sample after 2 MGT (see Fig. 9) in longitudinal and transversal woven directions – they can be compared to 28-day-old specimens					
AV fl. str. [MPa]	3.52	long.	AV fl. str. [MPa]	2.80	transv.
SD fl. str. [MPa]	0.27		SD fl. str. [MPa]	0.60	
Diff. from [18]	7.62		Diff. from [18]	21.64	
AV $y_{cent.}$ [mm]	2.07		AV $y_{cent.}$ [mm]	1.82	

In addition, it should be mentioned that the structural width of the CC is 1.1 m in the transversal direction and 73-200 m in the longitudinal direction, depending on the structural thickness.

In Fig. 15, the comparison of the flexural strengths of CC specimens and CC beams can be seen. The blue and orange columns mean the same specimens but in different weaving directions, while the grey columns represent the 4×4×16 cm^3 CC beams without the 3D fiber matrix.

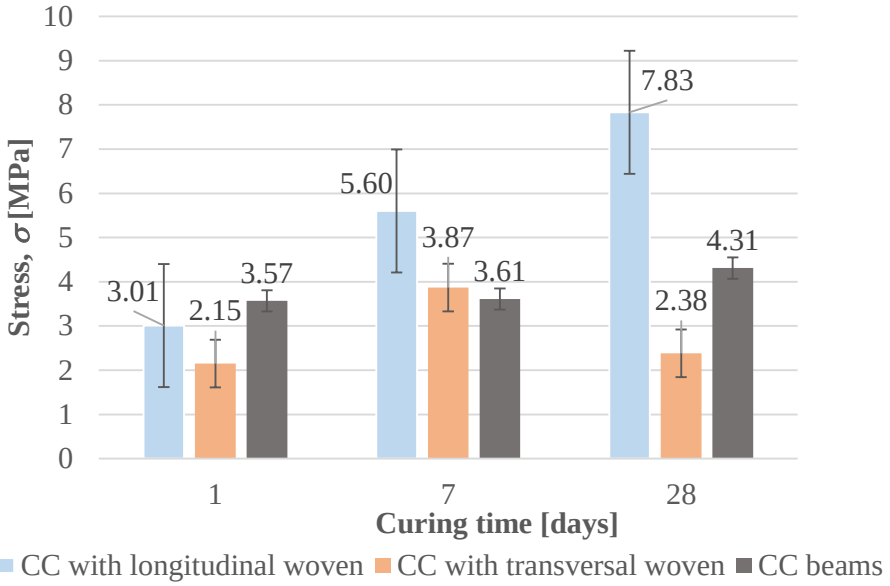

Fig. 15 Comparison of the flexural strengths of CC specimens in both weaving direction and CC beams, using the results from [18]

As can be seen, the standard deviation is considerable for the CC specimens but much smaller for the CC beams produced. This is probably due to the fact that in the former case, the hydration was not even, the waviness of the base material collecting water that cannot be absorbed immediately. When mixing the prepared beams, the material was evenly watered, while the bonding in the template was also done under equal conditions. As has been demonstrated so far, the weaving direction of the material has a significant influence on the flexural strength. The longitudinal weaving of CC provides a significant strength gain compared to the unreinforced condition, but this is not true for the transversely woven CC material. The flexural strength was close to the same or lower values compared to the unreinforced one. An exact summary of the reinforcement values is given in Table 4.

Table 4 compares the measured values for unreinforced and reinforced CC materials. Where the reinforced material did not show a higher value, it was marked as "ineffective". Overall, for longitudinal weaving, fiber reinforcement increased flexural strength by 55.1% after only 7 days of curing (from 3.61 to 5.60 MPa) and rose to 81.7% after 28 days of curing (from 4.31 to 7.83 MPa). Despite this, transversal weaving did not increase

proportionally. The reason for this can only be speculated. On the one hand, non-uniform hydration could have caused the discrepancy, and on the other hand, it is more likely, as was already apparent from the original measurements, that the transversal weaving is much weaker. As mentioned, the transversal direction length is 1.1 m, while the longitudinal direction can be 73-200 m (depending on the type of material). Therefore, based on the authors' tests, it can be said that the flexural strength without fiber reinforcement is almost the same as the reinforced material for transversal weavings.

Table 4 The effect of the 3D reinforcement of the CCT3's flexural strength

Curing time	**CC non-reinforced**	**CC with 3D fibre – longitudinal woven**		**CC with 3D fibre – transversal woven**	
	AV fl. str. [MPa]	AV fl. str. [MPa]	Increase [%]	AV fl. str. [MPa]	Increase [%]
1 day	3.57	3.01	not affect	2.15	not affect
7 days	3.61	5.60	55.1%	3.87	7.2%
28 days	4.31	7.83	81.7%	2.38	not affect

In Fig. 16, the flexural strengths of CC specimens with flat surfaces and the CC specimens with deformed surfaces are compared. It was found that the results did not change significantly for the weaker transversal weaving, whereas the decrease was 4.31 MPa for the longitudinal weaving. The numerical comparison can be seen in Table 5. It is seen that the magnitude of the decrease is significant; however, as described in Section 3.1, the material still had sufficient cohesion after fracture, i.e., even in the case of possible cracking or fracture, drainage is not affected. Based on the experiences from the full-scale measurement, the decreased value is, therefore, tolerable in practical terms.

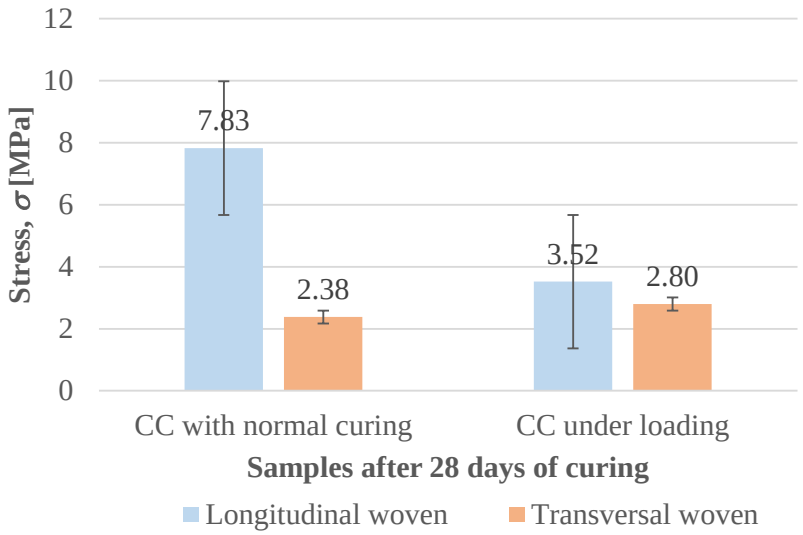

Fig. 16 Comparing flexural strength of the flat surface and the deformed surface CCs

Table 5 Comparison of the flexural strength of plain and deformed CC for both longitudinal and transversal weaving (bw. stand for 'between')

	CC specimens with a flat surface		**CC specimens from the full-scale test**	
	longitudinal woven	**transversal woven**	**longitudinal woven**	**transversal woven**
	curing time: 28 days			
AV strength [MPa]	7.83	2.38	3.52	2.80
Difference bw. long. wov. specimens [MPa]	–4.31			-
Difference bw. long. wov. specimens [%]	decreasing by 44.9%			-
Difference bw. tr. wov. specimens [MPa]	-	+0.42		
Difference bw. tr. wov. specimens [%]	-	increasing by 17.7%		

The subsequent measurement was the compression test of 4×4×4 cm^3 CC concrete blocks. This type of test was conducted to compare the results of the CC plates initially tested at 30×30×1.1 cm^3 dimension. That measurement was made to determine an adequate, usable Young's modulus. The process of analysis used the "least squares" method. A straight line was calculated that best fit the data, and then an array that described the line was returned [18]. The standard deviation was significant after the measurements. To ensure a proper comparison, the same evaluation was performed for the new specimens. It should be mentioned that the compression of the original specimens was affected by both the textile and the PVC layer and was not the case for the unreinforced cubes.

In Table 6, the relevant results of compression strength measurements are seen at 1-7-28 days of curing. It is seen that Young's modulus ratio (*YMR*) of the CC cube at 1 day is almost 10, while the 7 and 28-day specimens are almost 20. The difference is enormous, but it does not affect your experience of the product. Under 225 kN railway axle load, thanks to the load distribution, the distributed load on the subgrade surface is ~10 N/mm^2. From the results, it is seen that the material is capable of supporting the loads from the railway traffic and the track after any days of curing.

It is also seen that the compression strength at the CC cubes reached ~50% of the final strength, although this was measured with a relatively large standard deviation. This was below the value that characterizes the fast cure behavior of the material, which is 80% of the strength after one day of curing.

The results and the standard deviations are graphically presented in Fig. 17. The Young's modulus of CC specimens and CC cubes can be seen at 1-7-28 days of curing. By comparing the results of the CC material and the CC cube, it can be seen that the standard deviation is much smaller for the CC cube than for the CC specimen. The reason for this is the same as in the other study; the answer is hydration.

Table 6 Comparison of the flexural strength of plain and deformed CC for both long. and trans. woven with using of [18] – comp. means compression, *YMR* means Young's modulus ratio

	300×300×13 mm² CC specimens			**40×40×40 mm³ cubes without 3D fiber reinforcement**		
Curing	1 day	7 days	28 days	1 day	7 days	28 days
AV E [MPa]	480.70	515.50	523.60	4,548.12	10,161.42	10,737.76
SD E [MPa]	180.72	128.56	102.18	422.26	1,068.59	1,549.56
AV *YMR* [-]	-	-	-	9.46	19.71	20.51
AV comp. [mm]	1.08	0.81	0.97	0.91	0.63	0.65
SD comp. [mm]	0.36	0.15	0.06	0.20	0.17	0.11
AV $F_{V,max}$ [kN]	199.20 not broken	192.83 not broken	188.91 not broken	80.18 broken	112.51 broken	133.09 broken
SD $F_{V,max}$ [kN]	1.19	11.32	19.44	3.84	8.56	5.70
AV σ_{max} [MPa]	2.21 not broken	2.14 not broken	2.14 not broken	41.78	70.32	83.18
SD σ_{max} [MPa]	0.01	0.13	0.22	20.61	5.35	3.57

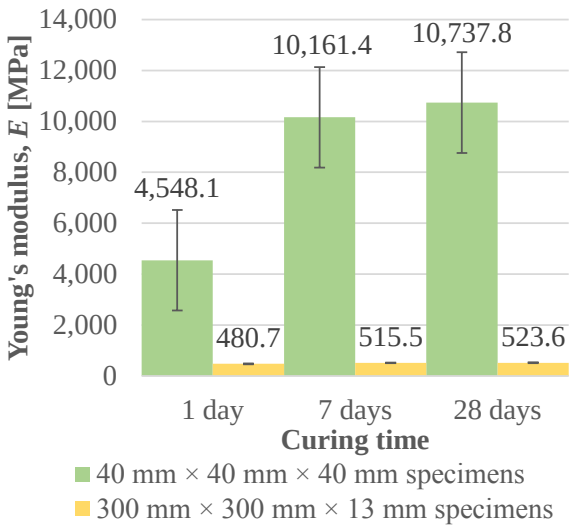

Fig. 17 Comparing compression strength of the 300×300×13 mm³ CC specimen and the 40×40×40 mm³ CC cubes using the results from [18]

After evaluating the results, it was concluded that the evaluated Young's modulus of the 3D fiber reinforcement is significantly weaker due to the dense weaving. The fiber reinforcement strengthens the CC material for some measurements and also weakens it for some measurements. All this is a scientific approach; the practical use of this fact does not change because its relatively thin design and its flexible laying on the ground improves its functionality.

For these reasons, although the measurements give the reader a good picture, the use of the results in modeling did not yield the same results when comparing the modeling of the different tests. It can be seen that the 3D fiber reinforcement and the double-sided overlay only allow the material to be tested as a complex composite structure and that the reinforcement has different effects on the resistances encountered in each test. The fiber reinforcement apparently weakens the material so much that the middle of the layer cannot be taken as one material in modeling. In summary, if someone wants to model with the CC material, one would need to define 4 material relationships to get valid values. For these reasons, data from CC tests without reinforcement, although showing the extent of reinforcement, are still insufficient for FE modeling.

4. CONCLUSIONS

The main question of this paper was whether CC can be applied under real-scale dynamic railway loads. According to the results, this study highlights the significant advantages of using CC to renew local failures and improve the lifetime of the railway track.

The authors examined the deformation of the surface with a flatness test and found that the surface is continuous, and no fracture is visible. After that, the material was cut, which was used for a deflection test. With the deflection test, it was found that, due to the fiber structure, the CC layer is more of a semi-rigid material than a rigid one. Although the first crack or fracture occurred at a deflection of 1-3 mm – after loading up to a deflection of 9-10 mm – the material returns to a deflection of 3-4 mm in a resting state. During this time, micro-fractures occurred in the structure, but the surface remained "intact".

Its quasi-rigid behavior under cyclic loading halved settlement compared to unreinforced tracks after one million load cycles. Moreover, CC proved durable, maintaining its structural integrity and cohesion under prolonged dynamic loading with no signs of significant cracking or failure. Key performance metrics, such as flatness and shear resistance, underscored its robustness, while its drainage properties and enhanced shear resistance (achieved through preloading) reduced risks associated with weak subgrades and poor water management.

It was also seen that the 3D reinforcement in the CC significantly increases the flexural strength in the longitudinal weaving direction, while the effect in the transversal direction is not relevant. Fiber reinforcement, particularly with longitudinal weaving, significantly enhances the flexural strength of cement composite materials, with a 55.1% increase after 7 days and an 81.7% increase after 28 days of curing. These improvements highlight the effectiveness of fiber reinforcement in enhancing the mechanical properties of CC materials over time.

The dense distribution of the 3D matrix structure led to a significant property reduction in the CC, causing the material's elastic modulus to decrease by a factor of 10-20 compared

to the non-reinforced version. However, other tests indicate that, with adequate plane support, the material is capable of withstanding railway loads without substantial damage.

Based on these variable results, it is clear why previous models could not be adequately validated. The four materials of the CC layer should be modeled as composite layers, but due to their varying design and hydration, deriving valid values for other types of modeling is challenging.

Basically, the technology is less economical in the case of new construction due to the high cost of materials. In the authors' opinion, the application of the material is suitable for repairing local defects, or it can be attached to a screening machine and "pulled" under the crushed stone ballast, similar to the geotextile and/or geogrids in rolls. Based on these experiences, different options and layer structures should be determined in the future.

This study identified some limitations. Variations in material thickness and weaving influenced performance, pointing to the need for standardized manufacturing processes. Additionally, the controlled hydration conditions used in the laboratory might not fully replicate real-world field scenarios, potentially affecting the material's performance in practice. The research also focused mainly on static and cyclic loads, leaving other factors, such as extreme temperatures and chemical exposure, unexplored.

Future research should emphasize field testing and long-term monitoring to evaluate CC's performance in diverse environmental and operational settings. Advanced finite element modeling could provide deeper insights into its behavior under complex loading scenarios, such as high-speed rail traffic and impact forces. Exploring alternative material compositions, including enhanced fiber reinforcements or hybrid composites, may further improve its flexibility and load distribution properties.

In conclusion, this study establishes CC as an auspicious material for reinforcing railway substructures with local failures. With further innovation, field validation, and development of its material properties, CC has the potential to expand its applications in railway infrastructure.

Acknowledgement: *This paper received technical support from the research team "SZE-RAIL." Special gratitude is extended to Dr. Szabolcs Szalai, Brigitta Fruzsina Szívós, Hanna Csótár, and Vivien Nemes, all affiliated with Széchenyi István University (SIU), for their invaluable assistance in performing the GOM measurements and evaluations. Acknowledgments are also due to Dr. Majid Movahedi Rad, Dr. Attila Németh, Dr. Dániel Harrach, Gusztáv Baranyai, and Erika Huschek-Juhász, also from Széchenyi István University (SIU), for their significant contributions to the execution of laboratory tests. The authors appreciate the technical and moral support provided by So De Go Consulting Ltd., led by CEO György Bozi, as well as Concrete Canvas Ltd. for their assistance in the procurement, delivery, and logistics of the CC samples from Hungary and the UK. The related investigations were conducted in the Building Materials and Structural Testing Laboratory (SIU, Faculty of Architecture, Civil Engineering and Transport Sciences) and the 3D Surface Digitization and Length Measurement Technology Laboratory (SIU, Audi Hungaria Faculty of Automotive Engineering). The English language proofreading of the article was carried out by Bettina Gerencsér. This research was conducted as part of the SIU Foundation's project titled 'Sustainable railways – Investigation of the energy efficiency of electric rail vehicles and their infrastructure'.*

REFERENCES

1. Ézsiás, L., Tompa, R., Fischer, S., 2024, *Investigation of the possible correlations between specific characteristics of crushed stone aggregates*, Spectrum of Mechanical Engineering and Operational Research, 1(1), pp. 10-26.
2. Kuchak, A.T.J., Marinkovic, D., Zehn, M., 2021, *Parametric investigation of a rail damper design based on a lab-scaled model*, Journal of Vibration Engineering & Technologies, 9, pp. 51-60.
3. Kuchak, A.T.J., Marinkovic, D., Zehn, M., 2020, *Finite element model updating—Case study of a rail damper*, Structural Engineering and Mechanics, 73(1), pp. 27-35.
4. Kampczyk, A., Dybeł, K., 2021, *The fundamental approach of the digital twin application in railway turnouts with innovative monitoring of weather conditions*, Sensors, 21(17), 5757.
5. Fischer, S., 2025, *Investigation of the Settlement Behavior of Ballasted Railway Tracks Due to Dynamic Loading*, Spectrum of Mechanical Engineering and Operational Research, 2(1), pp. 24-46.
6. Fischer, S., Harangozó, D., Németh, D., Kocsis, B., Sysyn, M., Kurhan, D., Brautigam, A., 2024, *Investigation of heat-affected zones of thermite rail weldings*, Facta Universitatis, Series: Mechanical Engineering, 22(4), pp. 689-710.
7. Alsirawan, R., Koch, E., 2024, *Dynamic Analysis of Geosynthetic-reinforced Pile-supported Embankment for a High-Speed Rail*, Acta Polytechnica Hungarica, 21(1), pp. 31-50.
8. Lovska, A., Gerlici, J., Dižo, J., Ishchuk, V., 2023, *The strength of rail vehicles transported by a ferry considering the influence of sea waves on its hull*, Sensors, 24(1), 183.
9. Semenov, S., Mikhailov, E., Kovtanets, M., Sergienko, O., Dižo, J., Blatnický, M., Gerlici, J., Kostrzewski, M., 2023, *Kinematic running resistance of an urban rail vehicle undercarriage: a study of the impact of wheel design*, Scientific Reports, 13(1), 10856.
10. Volkov, V., Taran, I., Volkova, T., Pavlenko, O., Berezhnaja, N., 2020, *Determining the efficient management system for a specialized transport enterprise*, Naukovyi Visnyk Natsionalnoho Hirnychoho Universytetu, 2020(4), pp. 185-191.
11. Saukenova, I., Oliskevych, M., Taran, I., Toktamyssova, A., Aliakbarkyzy, D., Pelo, R., 2022, *Optimization of schedules for early garbage collection and disposal in the megapolis*, Eastern-European Journal of Enterprise Technologies, 1(3(115)), pp. 13-23.
12. Ficzere, P., 2023, *The role of artificial intelligence in the development of rail transport*, Cognitive Sustainability, 2(4), 81.
13. Kampczyk, A., Gamon, W., Gawlak, K., 2023, *Integration of Traction Electricity Consumption Determinants with Route Geometry and Vehicle Characteristics*, Energies, 16(6), 2689.
14. Dmitriev, S.V., Morkina, A.Y., Tarov, D.V., Khalikova, G.R., Abdullina, D.U., Tatarinov, P.S., Semenov, A.S., Naimark, O.B., Khokhlov, A.V., Stolyarov, V.V., 2024, *Effect of Repetitive High-Density Current Pulses on Plastic Deformation of Copper Wires under Stepwise Loading*, Spectrum of Mechanical Engineering and Operational Research, 1(1), pp. 27-43.
15. Concrete Canvas Ltd., 2024, *Official website of Concrete Canvas*, Retrieved from: https://www.concretecanvas.com (last access: 10.12.2024).
16. Eller, B., Szalai, S., Sysyn, M., Harrach, D., Liu, J., Fischer, S., 2023, *Inner shear resistance increasing effect of Concrete Canvas in ballasted railway tracks*, Naukovyi Visnyk Natsionalnoho Hirnychoho Universytetu, 2023(2), pp. 64-70.
17. Eller, B., Szalai, S., Sysyn, M., Harrach, D., Liu, J., Fischer, S., 2024, *Advantages of using Concrete Canvas materials in railway track construction*, Naukovyi Visnyk Natsionalnoho Hirnychoho Universytetu, 2024(1), pp. 50-57.
18. Eller, B., Movahedi Rad, M., Fischer, S., 2022, *Laboratory Tests and FE Modeling of the Concrete Canvas, for Infrastructure Applications*, Acta Polytechnica Hungarica, 19(3), pp. 9-20.
19. Fischer, S., 2015, *Investigation of inner shear resistance of geogrids built under granular protection layers and railway ballast*, Nauka ta Progres Transportu, 59(5), pp. 97-106.
20. Al-Sumaiday, H., Khalaf, W.D., Muhauwiss, F.M., 2024, *Experimental Investigation of Bearing Capacity of Circular and Ring Footings on Geogrid-Reinforced Cohesionless Soils*, Civil and Environmental Engineering, 20(1), pp. 349-363.
21. Indraratna, B., Rujikiatkamjorn, C., Salim, W., 2023, *Advanced rail geotechnology–ballasted track, 2nd edition*, CRC Press, London, UK, 466 p.
22. Roshan, M.J., Rashid, A.S.A., Wahab, N.A., Tamassoki, S., Jusoh, S.N., Hezmi, M.A., Nik Norsyahariati, N.D., Nazirah, M.A., Mastura, A., 2022, *Improved methods to prevent railway embankment failure and subgrade degradation: A review*, Transportation Geotechnics, 37, 100834.
23. Liu, X., Xiao, J., Cai, D., Su, Q., Yang, G., Yuan, S., Jiang, G., 2023, *Recent advances in subgrade engineering for high-speed railway*, Intelligent Transportation Infrastructure, 2, liad001.

24. Le Kouby, A., Guimond-Barrett, A., Reiffsteck, P., Pantet, A., Mosser, J.F., Calon, N., 2020, *Improvement of existing railway subgrade by deep mixing*, European Journal of Environmental and Civil Engineering, 24(8), pp. 1229-1244.
25. Fortunato, E., Paixão, A., Morais, P., Santos, C., Morais, J., Cruz, J., Cruz, N., 2021, *Subgrade reinforcement of old railway tracks using short soil–binder columns – Laboratory studies and field tests*, Transportation Geotechnics, 29, 100577.
26. Solihu, H., 2020, *Cement soil stabilization as an improvement technique for rail track subgrade, and highway subbase and base courses: A review*, Journal of Civil and Environmental Engineering, 10(3), 1-6.
27. Liu, S., Ma, X., Ma, Y., Chen, Z., Dong, Z., Ma, P., 2023, *Review on the design and application of Concrete Canvas reinforced with spacer fabric*, Journal of Engineered Fibers and Fabrics, 18, 15588250231152591.
28. Zhao, T., Long, H., Yang, T., Liu, Y., 2018, *Cushioning properties of weft-knitted spacer fabrics*, Textile Research Journal, 88(14), pp. 1628-1640.
29. Liu, Y., Hu, H., Zhao, L., Long, H., 2012, *Compression behavior of warp-knitted spacer fabrics for cushioning applications*, Textile Research Journal, 82(1), pp. 11-20.
30. Ghorbani, V., Jeddi, A.A.A., Dabiryan, H., Ramezanianpour, A.A., 2020, *Investigation of the flexural behavior of self-consolidating mortars reinforced with net warp-knitted spacer fabrics*, Construction and Building Materials, 232, 117270.
31. Ko, E., Lee, H., Nam, K., Jeon, H.Y., 2024, *A study on GCCM (geosynthetic cementitious composite mat) performance improvement by structural composition of woven geotextiles*, E3S Web of Conferences, 569, 24003.
32. Jun, Z., Wei, X., Xingzhong, W., Peiwei, G., Zhihua, Y., Lihai, S., Jiang, W., 2020, *Application and research status of Concrete Canvas and its application prospect in emergency engineering*, Journal of Engineered Fibers and Fabrics, 15, 1558925020975759.
33. Mohammadsalehi, A., Mostofinejad, D., 2023, *Behavior of high-performance Concrete Canvas Miura-origami structures under flexural loading*, Structures, 54, pp. 928-945.
34. Wang, J., Xiang, Z.H., Niu, J.G., Li, J.J., Xu, W.M., 2023, *Mechanical properties of short concrete columns reinforced with carbon fiber reinforced composite strips and Concrete Canvas under axial compression based on acoustic emission*, Structures, 49, pp. 365-376.
35. Xiang, Z., Wang, J., Niu, J., Zhou, J., Wang, J., 2023, *Experimental study on the mechanical properties of Concrete Canvas and CFRP jointly confined circular concrete columns under axial compression*, Construction and Building Materials, 385, 130800.
36. Jafari, Z., Mostofinejad, D., 2024, *Flexural strengthening of RC beams by advanced Concrete Canvas*, Structural Concrete, 25(2), pp. 1165-1184.
37. American Society for Testing and Materials, 2018, ASTM D8173-18, *Standard guide for site preparation, layout, installation, and hydration of geosynthetic cementitious composite mats*, 8 p.
38. American Society for Testing and Materials, 2019, ASTM D8058-19, *Standard test method for determining the flexural strength of a geosynthetic cementitious composite mat (GCCM) using the three-point bending test*, 6 p.
39. American Society for Testing and Materials, 2020, *ASTM D8329-21, Standard test method for determination of water/cementitious materials ratio for geosynthetic cementitious composite mats (GCCMs) and measurement of the compression strength of the cementitious material contained within*, 3 p.
40. Hungarian Standards Institute, 2003, *MSZ EN 13450:2003, Aggregates for railway ballast*, 33 p.
41. Hungarian Standards Institute, 2012, *MSZ EN 933-1:2012, Tests for geometrical properties of aggregates. Part 1: Determination of particle size distribution. Sieving method*, 19 p.
42. Szalai, S., Czinege, I., 2017, *Digital image analysis of sheet metal testing and forming*, Proceedings of the 15th IMEKO TC10 Workshop on Technical Diagnostics in Cyber-Physical Era, Budapest, pp. 176-180.
43. Kocsis Szürke, S., Szalai, S., Lakatos, I., 2020, *Battery deformation measurement with DIC technique*, Proceedings of the 21st International Symposium on Electrical Apparatus & Technologies (SIELA), Bourgas, 91671092.
44. Szalai, S., Harangozó, D., Czinege, I., 2020, *Characterisation of inhomogeneous plastic deformation of AlMg sheet metals during tensile tests*, IOP Conference Series: Materials Science and Engineering, 903(1), 012023.
45. Kocsis Szürke, S., Dineva, A., Szalai, S., Lakatos, I., 2022, *Determination of critical deformation regions of a lithium polymer battery by DIC measurement and WOWA filter*, Acta Polytechnica Hungarica, 19(2), pp. 113-134.
46. Szalai, S., Dogossy, G., 2021, *Speckle pattern optimization for DIC technologies*, Acta Technica Jaurinensis, 14(3), pp. 228-243.
47. Szalai, S., Szívós, B.F., Kocsis, D., Sysyn, M., Liu, J., Fischer, S., 2024, *The Application of DIC in Criminology Analysis Procedures to Measure Skin Deformation*, Journal of Applied and Computational Mechanics, 10(4), pp. 817-829.

48. Szalai, S., Harangozó, D., Czinege, I., 2019, *Characterisation of Diffuse and Local Necking of Aluminium Alloy Sheets Using DIC Technique*, Acta Technica Jaurinensis, 12(3), pp. 191-204.
49. Szalai, S., Eller, B., Juhász, E., Movahedi Rad, M., Németh, A., Harrach, D., Baranyai, G., Fischer, S., 2022, *Investigation of deformations of ballasted railway track during collapse using the Digital Image Correlation Method (DICM)*, Reports in Mechanical Engineering, 3(1), pp. 258-282.
50. Hungarian Standards Institute, 1989, *MSZ 2509-3:1989, Bearing capacity test on pavement structures. Plate bearing test*, 6 p.
51. Redaelli, D.F., Barsanti, S.G., Biffi, E., Storm, F.A., Colombo, G., 2021, *Comparison of geometrical accuracy of active devices for 3D orthopaedic reconstructions*, The International Journal of Advanced Manufacturing Technology, 114(1), pp. 319-342.
52. GOM, 2011, *GOM ATOS III Triple Scan User Manual*, https://www.manualslib.com/products/Gom-Atos-Iii-Triple-Scan-10970231.html (last access: 10.12.2024).
53. GOM, 2021, *ATOS Compact Scan*, https://www.gom.com/en/products/3d-scanning/atos-compact-scan (last access: 10.12.2024).
54. Fischer, S., 2017, *Breakage test of railway ballast materials with new laboratory method*, Periodica Polytechnica Civil Engineering, 61(4), pp. 794-802.
55. Jongvivatsakul, P., Ramdit, T., Ngo, P.T., Likitlersuang, S., 2019, *Experimental investigation on mechanical properties of geosynthetic cementitious composite mat (GCCM)*, Construction and Building Materials, 166, pp. 956-965.
56. Zhang, F., Chen, H., Li, X., Li, H., Lv, T., Zhang, W., Yang, Y., 2017, *Experimental study of the mechanical behavior of FRP-reinforced Concrete Canvas panels*, Composite Structures, 176, pp. 608-616.
57. Han, F., Chen, H., Jiang, K., Zhang, W., Lv, T., Yang, Y., 2014, *Influences of geometric patterns of 3D spacer fabric on tensile behavior of Concrete Canvas*, Construction and Building Materials, 65, pp. 620-629.
58. Han, F., Chen, H., Li, X., Bao, B., Lv, T., Zhang, W., Hui Duan, W., 2015, *Improvement of mechanical properties of Concrete Canvas by anhydrite-modified calcium sulfoaluminate cement*, Journal of Composite Materials, 50(14), pp. 1937-1950.
59. Han, F., Chen, H., Zhang, W., Lv, T., Yang, Y., 2016, *Influence of 3D spacer fabric on drying shrinkage of Concrete Canvas*, Journal of Industrial Textiles, 45(6), pp. 1457-1476.
60. Hungarian Standards Institute, 2017, *MSZ EN 206:2013+A1:2017, Concrete. Specification, performance, production, and conformity*, 103 p.